Inorganic Chemistry
Article

Inorg. Chem. 2009, 48, 8709–8717 8709
DOI: 10.1021/ic9007119

^{91}Zr Nuclear Magnetic Resonance Spectroscopy of Solid Zirconium Halides at High Magnetic Field

O. Pauvert,[†,‡] F. Fayon,[*,†,‡] A. Rakhmatullin,[†,‡] S. Krämer,[§] M. Horvatić,[§] D. Avignant,[∥] C. Berthier,[§] M. Deschamps,[†,‡] D. Massiot,[†,‡] and C. Bessada[†,‡]

[†]*CEMHTI, CNRS UPR 3079, 1D avenue de la recherche scientifique, 45071 Orléans cedex 2, France,* [‡]*Université d'Orléans, Faculté des Sciences, avenue du Parc Floral, BP 6749, 45067 Orléans cedex 2, France,* [§]*Laboratoire National des Champs Magnétiques Intenses (LNCMI), CNRS UPR 3228, BP 166, 25 rue des Martyrs, 38042 Grenoble cedex 9, France, and* [∥]*Laboratoire des Matériaux Inorganiques, CNRS UMR 6002, Université Blaise Pascal, 24 avenue des Landais, 63177, Aubière cedex, France*

Received April 10, 2009

^{91}Zr solid-state NMR spectra of zirconium halides and several fluorozirconates have been obtained at high magnetic fields up to 30 T using both the Hahn-Echo and the Quadrupolar Carr−Purcell−Meiboom−Gill sequences combined with the broadband Variable Offset Cumulative Spectrum technique. For the zirconium halides, the ^{91}Zr isotropic chemical shift covers a range of about 2000 ppm and shows a good correlation with Pauling's electronegativity and ionic potential of the halogen. For the fluorozirconate samples, in which the Zr atoms exhibit various coordination polyhedra, increasing the Zr coordination number and the mean Zr−F bond length leads to an increased isotropic shielding. In the studied compounds the ^{91}Zr quadrupolar coupling constants (C_Q's) range from 10.6 to 44.7 MHz. For 6-fold coordinated Zr sites, a correlation between C_Q and the shear strain of the octahedron is observed, and we investigate the relationship between the C_Q and the distortion of the polyhedron for 8-fold coordinated Zr sites using different distortion criteria.

1. Introduction

Zirconium is known to have a wide range of industrial applications from jewelry to nuclear energy. For example, various zirconium oxides such as zircon ($ZrSiO_4$) or zirconia (ZrO_2) are used as crystal substitute for diamonds, or for furnace equipments and ceramics applications. ZrF_4 is also one of the main constituents of optical fibers. Because of their resistance to corrosion at high temperature, zirconium based-materials are extensively used in chemical industry as high temperature refractories or for piping in corrosive environments, especially for nuclear technology. In addition, zirconium atom has a low capture cross section for thermal neutrons and is well adapted as cladding for nuclear fuel rods, usually as zirconium alloy (Zircaloy). The improvement of these different materials for their specific applications requires a precise knowledge of the zirconium local structure and a better description of its structural configuration.

Solid-state Nuclear Magnetic Resonance (NMR) spectroscopy has proved to be a powerful tool in elucidating the local environment of atoms in complex crystalline or disordered materials.[1,2] However, ^{91}Zr solid-state NMR spectroscopy remains challenging because ^{91}Zr has a relatively low natural abundance (11.23%) and a low gyromagnetic ratio (3.958 MHz T^{-1}). In addition, ^{91}Zr has a nuclear spin $I = 5/2$ associated with a large nuclear quadrupole moment[3] (-0.176×10^{-28} m^2) and is therefore subject to strong quadrupolar interactions leading to very broad powder NMR spectra. Usually, even at high magnetic fields, only the $\langle 1/2, -1/2 \rangle$ central transition is observable and spreads over hundreds of kHz.[4−16]

*To whom correspondence should be addressed. E-mail: franck.fayon@cnrs-orleans.fr.

(1) Eckert, H. *Prog. Nucl. Magn. Reson. Spectrosc.* **1992**, *24*, 159–293.
(2) MacKenzie, K. J. D.; Smith, M. E. *Multinuclear Solid-State NMR of Inorganic Materials*; Pergamon: Amsterdam, 2002.
(3) Kellö, V.; Pyykkö, P.; Sadlej, A. J.; Schwerdtfeger, P.; Thyssen, J. *Chem. Phys. Lett.* **2000**, *318*, 222–231.
(4) Bastow, T. J. *J. Phys.: Condens. Matter* **1990**, *2*, 6327–6330.
(5) Hartman, J. S.; Koffyberg, F. P.; Ripmeester, J. A. *J. Magn. Reson.* **1991**, *91*, 400–404.
(6) Bastow, T. J.; Smith, M. E.; Stuart, S. N. *Chem. Phys. Lett.* **1992**, *191*, 125–129.
(7) Bastow, T. J.; Smith, M. E.; Stuart, S. N. *Solid State NMR* **1992**, *1*, 165–174.
(8) Bastow, T. J.; Hobday, M. E.; Smith, M. E.; Whitfield, H. J. *Solid State Nucl. Magn. Reson.* **1996**, *5*, 293–303.
(9) Bastow, T. J.; Forwood, C. T.; Gibson, M. A.; Smith, M. E. *Phys. Rev. B* **1998**, *58*, 2988–2997.
(10) Bastow, T. J. *Z. Naturforsch.* **1994**, *49a*, 320–328.
(11) Hartmann, P.; Scheler, G. *Z. Naturforsch.* **1995**, *50a*, 90–94.
(12) Hung, I.; Schurko, R. W. *J. Phys. Chem. B.* **2004**, *108*, 9060–9069.
(13) Zhu, J.; Lin, Z.; Yan, Z.; Huang, Y. *Chem. Phys. Lett.* **2008**, *461*, 260–265.
(14) Yan, Z.; Kirby, C. W.; Huang, Y. *J. Phys. Chem. C* **2008**, *112*, 8575–8586.
(15) O'Dell, L. A.; Schurko, R. W. *Chem. Phys. Lett.* **2008**, *464*, 97–102.
(16) Tang, J. A.; O'Dell, L. A.; Aguiar, P. M.; Lucier, B. E. G.; Sakellariou, D.; Schurko, R. W. *Chem. Phys. Lett.* **2008**, *466*, 227–234.

Published on Web 08/14/2009

Hence, the Magic Angle Spinning (MAS) technique is not useful in this case and would give rise to much more complicated spectra because of the overlap of numerous second order broadened spinning sidebands.[17] Moreover, because of its high polarizability, zirconium is also subject to significant chemical shift anisotropy (CSA).[4,12,13]

Because of these difficulties, only few solid-state ^{91}Zr NMR studies have been reported up to now.[4−16] Solid-state ^{91}Zr NMR measurement was first performed by T. Bastow[4] in the case of zircon ($ZrSiO_4$) for which a quite large ^{91}Zr quadrupolar coupling constant (C_Q; C_Q = 20.5 MHz) associated with a significant CSA (−170 ppm) was determined from NMR single-crystal rotation patterns. ^{91}Zr NMR spectra recorded at a magnetic field of 9.4 T using a solid echo pulse sequence were further reported for various oxide materials ($BaZrO_3$, $SrZrO_3$, Ba_2ZrO_4, $ZrSiO_4$, ZrO_2, and ZrO_2 doped with CaO and MgO) showing the effect of the local site symmetry on the ^{91}Zr C_Q.[5] Following these works, quadrupole interaction parameters, Knight shifts, and chemical shifts were determined for Zr metal, ZrCo, ZrC, ZrH_2, monoclinic and tetragonal (3 mol % Y_2O_3) ZrO_2 from the analysis of ^{91}Zr static powder patterns.[6] In this case, both the frequency-stepped and the hard-pulse Hahn echo methods were used to record the very broad ^{91}Zr NMR spectra, showing that the former method allows obtaining spectra with clear edge singularities and preventing line shape distortion due to instrumental factors.[6] A relatively large ^{91}Zr C_Q was measured for the hexagonal close packed structure of zirconium metal (18.2 MHz) while vanishing C_Q values are reported for cubic ZrCo and cubic ZrC.[6] The link between crystal structure symmetry and C_Q's was also illustrated in ZrO_2 polymorphs, the C_Q of which is larger for the monoclinic form (23.1 MHz) than for the tetragonal one (19.1 MHz).[6,7] A C_Q of the same order of magnitude was found for a compound in the $Na_2O-ZrO_2-SiO_2$ ternary system (C_Q = 29.4 MHz),[8] while C_Q values of 7.3 and 53.7 MHz were measured for the Al_3Zr alloy[9] and ZrF_4,[10] respectively. ^{91}Zr NMR data were also reported for several zirconium phosphates, oxides, and fluorides having different site symmetries for which the ^{91}Zr C_Q values range from 330 kHz to 17.9 MHz.[11] More recently, ^{91}Zr solid-state NMR spectra of an organometallic zirconium complex (bis(cyclopentadienyl)-dichlorozirconium),[12] microporous zirconium silicate frameworks,[13] and layered zirconium phosphates[14] were also recorded using the Quadrupolar Carr−Purcell−Meiboom−Gill pulse sequence[18−20] (QCPMG). In these works, the QCPMG experiment, where trains of whole spin echoes are recorded, was used to significantly reduce the experimental time required to obtain ^{91}Zr spectra with good signal-to-noise ratio with respect to the Hahn echo sequence. The QCPMG sequence was also combined with adiabatic (broadband) pulses to record ^{91}Zr wide-line spectra of a ZrO_2 rotor[15] and sodium zirconate Na_2ZrO_3.[16]

In this work, we have collected ^{91}Zr solid-state NMR spectra of zirconium halides (β-ZrF_4, $ZrCl_4$, $ZrBr_4$, and ZrI_4) and of several alkali and alkaline earth fluorozirconates ($Na_5Zr_2F_{13}$, K_2ZrF_6, Cs_2ZrF_6, α-Ba_2ZrF_8) at high magnetic field (up to 30 T). The spectra were obtained using both the Hahn echo and QCPMG sequences combined with the broadband Variable Offset Cumulative Spectrum (VOCS)[17,21−23] technique. For all the studied compounds, ^{91}Zr chemical shift and quadrupolar coupling parameters were determined from analytical simulations of the powder patterns. To use ^{91}Zr NMR spectroscopy to probe the local environment of zirconium in more complex systems (zirconium based ceramics and glasses, high-temperature molten salts), relationships between structural parameters and both the ^{91}Zr isotropic chemical shift and the C_Q have been investigated. The influence of Pauling's electronegativity and ionic potential of the halogen, as well as Zr coordination number and mean Zr−F bond length, on the ^{91}Zr isotropic chemical shift is discussed. For the 6-fold and 8-fold coordinated Zr sites, correlations between the C_Q and polyhedra distortion criteria are also demonstrated.

2. Experimental Section

Zirconium chloride ($ZrCl_4$, 99.9% purity), zirconium bromide ($ZrBr_4$, 98% purity), and zirconium iodide (ZrI_4, 99.9% purity) were purchased from Sigma-Aldrich. A β-ZrF_4 sample of very high purity (99.99%) was provided by Dr. Pierre Chamelot (LGC, Toulouse). The $Na_5Zr_2F_{13}$, K_2ZrF_6, Cs_2ZrF_6, and α-Ba_2ZrF_8 were kindly provided by Dr. Pierre Florian (CEMHTI, Orléans). All samples were checked by powder X-rays diffraction. Because of the samples sensitivity to moisture, the sample containers were filled in a glove box under dried argon atmosphere.

^{91}Zr solid-state NMR experiment were performed using a Bruker Avance 750 spectrometer operating at a magnetic field of 17.6 T (^{91}Zr Larmor frequency of 69.7 MHz) with a 7 mm Bruker probehead and Si_3N_4 sample containers. For all experiments, the duration of the central-transition selective 90° pulse was 3 μs corresponding to a nutation frequency ω_1 of 83.3 kHz for the isolated central transition, and we have used recycle delays in the range 400−800 ms. The VOCS technique was used to reconstruct spectra broader than the excitation bandwidth of the radio frequency pulses. This technique consists in acquiring subspectra at different offsets, and summing them to reconstruct the broadband spectrum. A quasi uniform excitation over the required spectral range is achieved using offset step $\leq \omega_1$,[23] We have used a maximum offset step of 50 kHz, and the number of subspectra was adjusted depending on the span of the broadband spectrum. Five subspectra were recorded for $ZrCl_4$ while 43 subspectra were acquired for K_2ZrF_6. For each sample, the subspectra were recorded using two different pulse sequences: a Hahn echo with acquisition of the whole echo (which allows unambiguous phasing of the spectrum and improves the signal-to-noise ratio by a factor of up to $2^{1/2}$)[17] and the QCPMG[18−20] pulse sequence. The latter consists in acquiring trains of whole spin echoes, obtained by applying a series of equidistant 180° pulses. By adjusting the number of 180° pulses, the full coherence decay was recorded. The Fourier transform of the QCPMG echo-train provides a spectrum in the form of a set of equidistant spikelets defining the envelope of the broad spectrum. Alternatively, splitting the QCPMG echo-train into individual spin−echoes and making

(17) Massiot, D.; Farnan, I.; Gautier, N.; Trumeau, D.; Trokiner, A.; Coutures, J.-P. *Solid State Nucl. Magn. Reson.* **1995**, *4*, 241–248.
(18) Vosegaard, T.; Larsen, F. H.; Jakobsen, H. J.; Ellis, P. D.; Nielsen, N. C. *J. Am. Chem. Soc.* **1995**, *119*, 9055–956.
(19) Larsen, F. H.; Jakobsen, H. J.; Ellis, P. D.; Nielsen, N. C. *J. Phys. Chem. A* **1997**, *101*, 8597–8606.
(20) Larsen, F. H.; Jakobsen, H. J.; Ellis, P. D.; Nielsen, N. C. *J. Magn. Reson.* **1998**, *131*, 144–147.
(21) Fayon, F.; Landron, C.; Sakurai, K.; Bessada, C.; Massiot, D. *J. Non-Cryst. Solids* **1999**, *243*, 39–44.
(22) Clark, W. G.; Hanson, M. E.; Lefloch, F.; Ségransan, P. *Rev. Sci. Instrum.* **1995**, *66*, 2453–2464.
(23) Tong, Y. Y. *J. Magn. Reson. A* **1996**, *119*, 22–28.

the Fourier transform of the sum of these individual echoes allow directly recovering the broad static line shape. In comparison with the Hahn echo sequence, an increased sensitivity is obtained in reduced experimental time, depending on the ^{91}Zr transverse dephasing time constant (T_2') that defines the number of acquired echoes. For example, 20 and 40 spin−echoes with interpulse delays of 400 and 200 μs were recorded for Cs_2ZrF_6 and $Na_5Zr_2F_{13}$, respectively ($T_2' \sim 3.2$ ms), while 256 spin−echoes with an interpulse delay of 800 μs were acquired for $ZrCl_4$ ($T_2' \sim 105$ ms). The QCPMG subspectra were recorded with a number of transients 16 to 32 times smaller than that used to acquire the corresponding Hahn echo subspectra. It should be mentioned that the transverse coherence lifetime can be significantly lengthened using heteronuclear decoupling,[24] allowing to increase the number of acquired echoes and hence the sensitivity of the QCPMG experiment.[25,26] However, the spectra of the fluorozirconate samples, for which relatively short transverse dephasing times were observed, were recorded without ^{19}F decoupling using a single resonance 7 mm probehead. All experimental parameters used to record each VOCS spectrum with the Hahn echo and QCPMG sequences are given in the Supporting Information. ^{91}Zr chemical shifts were referenced relative to a saturated solution of $Zr(C_5H_5Cl)_2$ in CH_2Cl_2 at 0 ppm.[27]

For β-ZrF_4, a ^{91}Zr VOCS spectrum was also recorded at LNCMI-Grenoble in a magnetic field of 30 T using a 20 MW resistive magnet, a Tecmag NMR console, and a home-built broadband NMR probe tuned to 118.4 MHz. The duration of the central-transition selective 90° pulse was 2.5 μs, and seven subspectra were recorded with an offset step of 100 kHz to reconstruct the broadband spectrum. Because of the inhomogeneous field of the resistive magnet, the sample volume had to be reduced. A sample size of 4 mm in diameter and 6 mm in length was chosen as a compromise to keep the inhomogeneity of the external field below 100 ppm and to preserve at the same time the largest sample volume possible for sensitivity.

Analytical simulations of all spectra were performed using the dmfit software.[28] For β-ZrF4, ^{91}Zr quadrupolar and CSA parameters were obtained from a simultaneous fit of the static ^{91}Zr VOCS spectra recorded at two different magnetic fields of 17.6 and 30 T. For all other compounds, the parameters were determined by fitting simultaneously the Hahn echo VOCS spectrum and the QCPMG VOCS line shape, both recorded at 17.6 T. As already mentioned, QCPMG VOCS lineshapes were obtained by splitting the QCPMG echo-trains into individual spin−echoes and performing the Fourier transform of the sum of these individual echoes for each subspectrum. The errors in the simulations were determined using a Monte Carlo approach.[29−31] 500 data sets were generated from each Hahn echo VOCS spectrum and QCPMG VOCS line shape with added experimental noise and fitted using the same procedure. The standard deviations were used to estimate the uncertainties (2 times the standard deviation, corresponding to the 95% confidence limit).

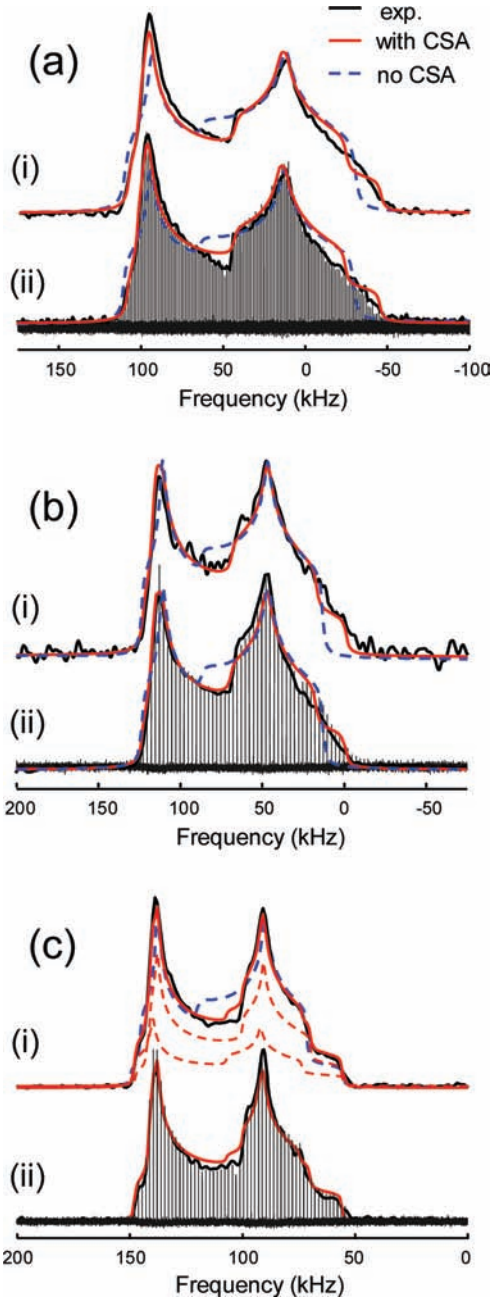

Figure 1. Experimental ^{91}Zr VOCS spectra recorded at 17.6 T using the Hahn echo (i) and QCPMG (ii) sequences of (a) $ZrCl_4$, (b) $ZrBr_4$, and (c) ZrI_4, and their analytical simulations with (red) and without CSA (dotted blue). The broad QCPMG line shape obtained by splitting the QCPMG echo-train into individual spin−echoes and making the Fourier transform of the sum of these individual echoes is shown on top of the spikelet spectrum.

3. Results

In Figures 1, 2, and 3, we show the broad ^{91}Zr static VOCS spectra of the zirconium halides and fluorozirconates that were recorded using both the Hahn echo and QCPMG sequences. As expected, these powder patterns show typical second order quadrupolar broadened line shapes. Because of

(24) De Paëpe, G.; Giraud, N.; Lesage, A.; Hodgkinson, P.; Böckmann, A.; Emsley, L. *J. Am. Chem. Soc.* **2003**, *125*, 13938–13939.
(25) Lipton, A. S.; Sears, J. A.; Ellis, P. D. *J. Magn. Reson.* **2001**, *151*, 48–59.
(26) Rossini, A. J.; Mills, R. W.; Briscoe, G. A.; Norton, E. L.; Geier, S. J.; Hung, I.; Zheng, S.; Autschbach, J.; Schurko, R. W. *J. Am. Chem. Soc.* **2009**, *131*, 3317–3330.
(27) Harris, R. K.; Becker, E. D.; Cabral de Menezes, S. M.; Goodfellow, R.; Granger, P. *Pure Appl. Chem.* **2001**, *73*, 1795–1818.
(28) Massiot, D.; Fayon, F.; Capron, M.; King, I.; Le Calvé, S.; Alonso, B.; Durand, J.-O.; Bujoli, B.; Gan, Z.; Hoatson, G. *Magn. Reson. Chem.* **2002**, *40*, 70–76.
(29) Cadars, S.; Lesage, A.; Hedin, N.; Chmelka, B. F.; Emsley, L. *J. Phys. Chem. B* **2006**, *110*, 16982–16991.
(30) Pham, T. N.; Griffin, J. M.; Masiero, S.; Lena, S.; Gottarelli, G.; Hodgkinson, P.; Filip, C.; Brown, S. P. *Phys. Chem. Chem. Phys.* **2007**, *9*, 3416–3423.
(31) Hiet, J.; Deschamps, M.; Pellerin, N.; Fayon, F.; Massiot, D. *Phys. Chem. Chem. Phys.* **2009**, *11*, 6935−6940.

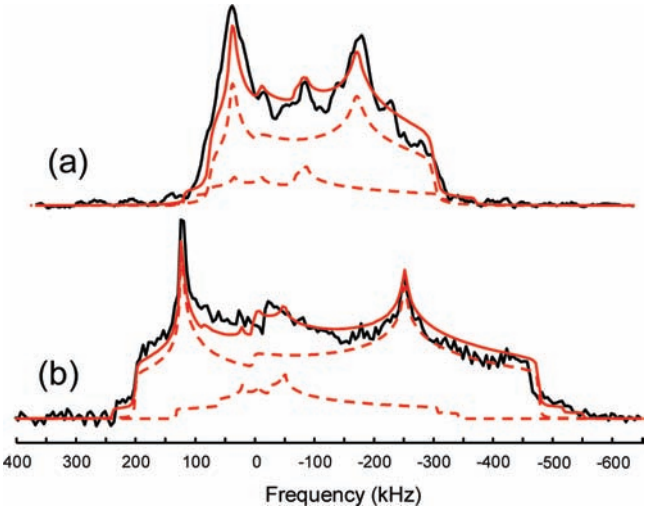

Figure 2. Experimental ^{91}Zr Hahn echo VOCS spectra of β-ZrF_4 recorded at 30 T (a) and 17.6 T (b) and their simulations.

its high polarizability (the highest of fourth row elements), zirconium is also subject to significant CSA,[4,12,13] which had often to be taken into account to obtain reliable fits of the experimental spectra. Second order quadrupolar effects and CSA are well-known to exhibit very different magnetic field dependences: the second order quadrupolar effects are scaled down when the principal magnetic field is increased while the CSA broadening increases proportionally to the magnetic field.[1,2] Owing to this contrasted magnetic field dependence of the CSA and quadrupolar broadening, the quadrupolar coupling and CSA parameters, as well as the three Euler angles specifying the relative orientation of the chemical shift and quadrupolar coupling tensors, can be determined from the simulations of a set of static powder spectra recorded at different magnetic fields.[32−34] However, determining these parameters from a single static spectrum remains difficult because of the complex interplay between them.

For β-ZrF_4, ^{91}Zr quadrupolar and CSA parameters were determined from a simultaneous simulation of the static ^{91}Zr VOCS spectra recorded at two different magnetic fields of 17.6 and 30 T. For the remaining samples, for which the static spectra were recorded at a single magnetic field, the quadrupolar and CSA parameters resulting from the best-fit spectrum are more ambiguous. For $Na_5Zr_2F_{13}$, K_2ZrF_6, Cs_2ZrF_6, and α-Ba_2ZrF_8, good fits of the ^{91}Zr experimental spectra can be obtained taking into account only the second order quadrupolar interaction, and including additional CSA did not improve the quality of the fits. In such cases, the ^{91}Zr CSA interaction cannot be reliably determined and was therefore neglected in the corresponding simulations. In contrast, attempts to fit the spectra of the $ZrCl_4$, $ZrBr_4$, and ZrI_4 samples with only a second order quadrupolar line shape have been unsuccessful, and the CSA interaction must be taken into account to obtain the best spectral simulations. For each of these three compounds, it must be pointed out that fits of similar qualities are reached for distinct CSA parameters and Euler angles, and that a unique set of CSA and quadrupolar parameters cannot be unambiguously determined from the simulation. Nevertheless, changing these parameters in the simulation affects only very slightly the ^{91}Zr isotropic chemical shift and quadrupolar coupling values which remain within their determined confidence intervals in all cases. The crystal structure data of the studied compounds are provided in Table 1 and the ^{91}Zr quadrupolar coupling and CSA parameters determined from spectral simulations are given in Table 2. The ^{91}Zr NMR spectra obtained for all samples are described below.

$ZrCl_4$ has a monoclinic structure built of edge-sharing $ZrCl_6$ octahedra forming infinite chains along the c axis (ISCD-26049).[35,36] The structure contains a single octahedral Zr site and two inequivalent chlorine sites. As depicted in Figure 1a, the ^{91}Zr static VOCS spectra of $ZrCl_4$ recorded using the Hahn echo and QCPMG sequences show a second-order quadrupolar line shape spanning over 150 kHz with well-defined singularities. The chemical shift and quadrupolar parameters determined by fitting the powder patterns are given in Table 2. As expected for a distorted $ZrCl_6$ octahedron far from axial symmetry, a significant C_Q value of 14.65 MHz with an asymmetry parameter η_Q of 0.48 is observed.

To our knowledge, crystallographic data of $ZrBr_4$ are surprisingly lacking in the literature. However, $ZrBr_4$ was stated to be isostructural with monoclinic $ZrCl_4$.[35,36] This is confirmed by our ^{91}Zr static (Hahn echo and QCPMG) VOCS spectra which show a quadrupolar line shape that is very similar to that observed for $ZrCl_4$ (see Figure 1b). The ^{91}Zr C_Q (C_Q = 13.16 MHz) and CSA (δ_{CSA} = 330 ppm) are slightly smaller for $ZrBr_4$ than for $ZrCl_4$ suggesting that the corresponding ZrX_6 octahedra are slightly less distorted.

The monoclinic structure of ZrI_4 is built of edge-sharing ZrI_6 octahedra forming infinite zigzag chains along the c axis (ICSD-8068).[37] The asymmetric unit contains two crystallographically inequivalent Zr sites of multiplicities 2 and 4 (for Zr1 and Zr2, respectively) and 6 inequivalent iodine sites. The ^{91}Zr static VOCS spectra only span over a 90 kHz frequency range indicating smaller C_Q values than those determined for $ZrCl_4$ or $ZrBr_4$ and therefore less distorted octahedra. Figure 1c shows the best fit of the powder pattern with two overlapping contributions of relative intensities in the ratio 1:2 accounting for the two different Zr sites. According to the site multiplicities, the broader resonance (C_Q = 11.00 MHz, δ_{ISO} = 1690 ppm) of lower intensity is assigned to Zr1, and the resonance of higher intensity is assigned to the Zr2 site (C_Q = 10.58 MHz, δ_{ISO} = 1667 ppm).

The monoclinic structure of β-ZrF_4 has been described as a three-dimensional network of corner-sharing ZrF_8 Archimedean antiprisms, in which each fluorine atom is coordinated by two zirconium atoms.[38] The structure contains seven inequivalent fluorine sites, which were previously evidenced by ^{19}F solid-state MAS NMR,[39] and two inequivalent

(32) Chu, P. J.; Gerstein, B. C. *J. Chem. Phys.* **1989**, *91*, 2081–2101.
(33) Cheng, J. T.; Edwards, J. C.; Ellis, P. D. *J. Phys. Chem.* **1990**, *94*, 553–561.
(34) Power, W. P.; Wasylishen, R. E.; Mooibroek, S.; Pettitt, B. A.; Danchura, W. *J. Phys. Chem.* **1990**, *94*, 591–598.
(35) Krebs, B. *Angew. Chem.* **1969**, *81*, 120–121.
(36) Krebs, B. *Z. Anorg. Allg. Chem.* **1970**, *378*, 263–272.
(37) Krebs, B.; Henkel, G.; Dartmann, M. *Acta Crystallogr. B* **1979**, *35*, 274–278.
(38) Burbank, R. D.; Bensey, F. N. *J. USAEC Rep.* **1956**, *K-1280*, 1–19.
(39) Legein, C.; Fayon, F.; Martineau, C.; Body, M.; Buzaré, J.-Y.; Massiot, D.; Durand, E.; Tressaud, A.; Demourgues, A.; Péron, O.; Boulard, B. *Inorg. Chem.* **2006**, *45*, 10636–10641.

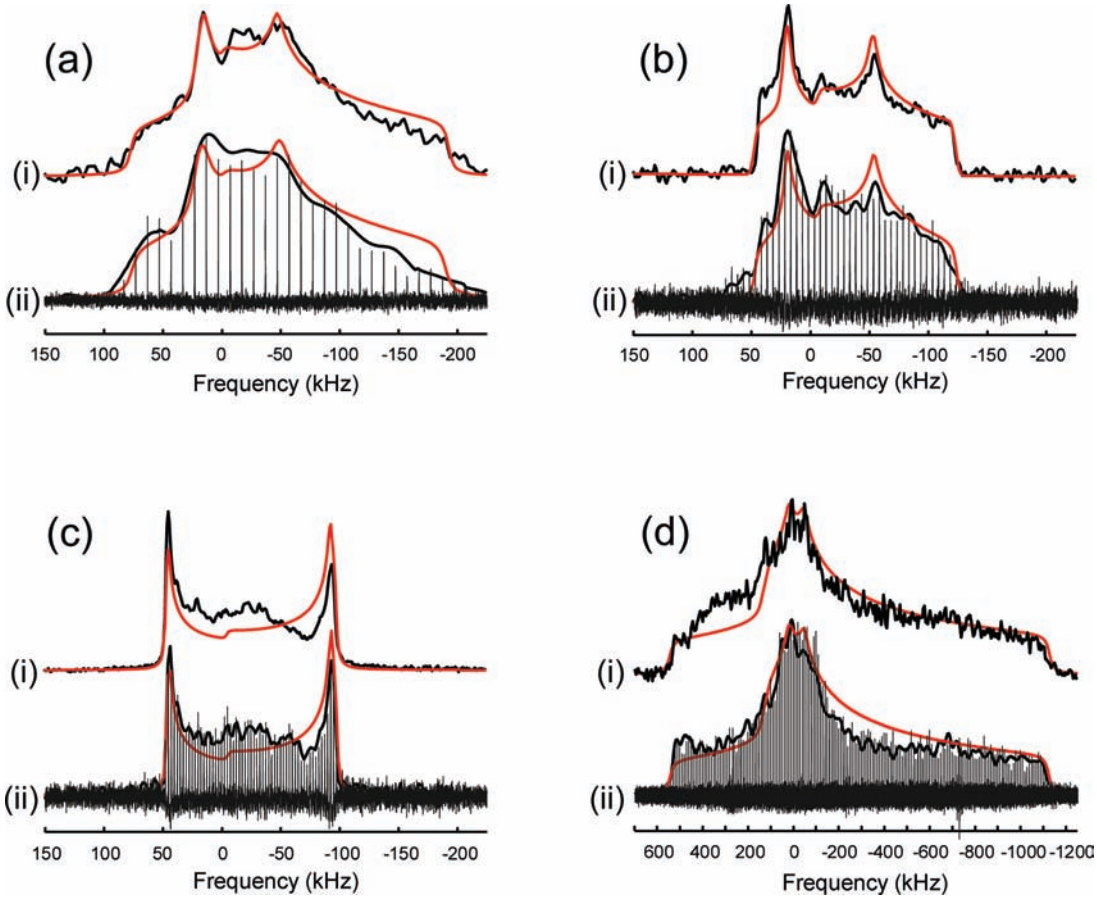

Figure 3. Experimental ^{91}Zr VOCS spectra recorded at 17.6 T using the Hahn echo (i) and QCPMG (ii) sequences of (a) α-Ba_2ZrF_8, (b) $Na_5Zr_2F_{13}$, (c) Cs_2ZrF_6, and (d) K_2ZrF_6, and their simulations without CSA (red). The broad QCPMG line shape obtained by splitting the QCPMG echo-train into individual spin−echoes and making the Fourier transform of the sum of these individual echoes is shown on top of the spikelet spectrum.

Table 1. Crystallographic Data of the Zirconium Compounds[a]

compounds	unit cell parameters (Å)	space group	Zr coordination number (CN)	Zr coordination polyhedra	average Zr−X bond length (Å)	$\|\alpha\|$	$\|\psi\|$
$ZrCl_4$	$a = 6.361$, $b = 7.407$, $c = 6.256$, $\beta = 109.30°$	$P2/c$	6	O	Zr−Cl = 2.49	0.300	1.313
ZrI_4	$a = 8.356$, $b = 8.326$, $c = 17.926$, $\beta = 103.21°$	$P2/c$	6 (Zr1)	O	Zr1−I = 2.86	0.247	1.102
			6 (Zr2)	O	Zr2−I = 2.86	0.262	1.057
β-ZrF_4	$a = 9.57$, $b = 9.93$, $c = 7.73$, $\beta = 94.28°$	$I2/c$	8 (Zr1)	AA	Zr1−F = 2.08		
			8 (Zr2)	BTP	Zr2−F = 2.12		
α-Ba_2ZrF_8	$a = 9.743$, $b = 5.616$, $c = 11.888$	Pnma	8	BTP	Zr−F = 2.12		
$Na_5Zr_2F_{13}$	$a = 11.62$, $b = 5.49$, $c = 8.44$, $\beta = 97.72°$	$P2_1/c$	7	MTP	Zr−F = 2.09		
Cs_2ZrF_6	$a = 6.410$, $c = 5.010$	$P\bar{3}$m1	6	O	Zr−F = 2.04	0.070	1.739
K_2ZrF_6	$a = 6.582$, $b = 11.442$, $c = 6.942$	$C2/c$	8	AA	Zr−F = 2.11		

[a] O: Octahedron, AA, Archimedean Antiprism, BTP: Bicapped Trigonal Prism, MTP: Monocapped Trigonal Prism.

Zr crystallographic sites of multiplicities 4 and 8 (for Zr1 and Zr2, respectively). According to the Porai-Koshits and Aslanov's criteria,[40] the Zr1 coordination polyhedron is clearly identified as an Archimedean antiprism while the Zr2 coordination polyhedron is better described as a bicapped trigonal prism. As shown in Figure 2, the ^{91}Zr static VOCS spectrum recorded with a Hahn echo sequence at 17.6 T is very broad, spanning over a frequency range of ∼700 kHz. Extracting the parameters of the two expected ^{91}Zr contributions from only this single spectrum remains difficult. Therefore, a ^{91}Zr static VOCS spectrum was recorded at a higher magnetic field of 30 T to help separating the two contributions. As expected, the span of the spectrum acquired at 30 T is reduced by a factor of 1.7 because of the scaling effect of the principal field on the second order quadrupolar broadening.

(40) Porai-Koshits, M. A.; Aslanov, L. A. *J. Struct. Chem.* **1972**, *13*, 244–253.

Table 2. ^{91}Zr Isotropic Chemical Shift (δ_{ISO}), C_Q, Asymmetry Parameter of the Quadrupolar Coupling Tensor (η_Q), Chemical Shift Anisotropy (δ_{csa}), Asymmetry Parameter of the Chemical Shift Tensor (η_{CSA}), and Euler Angles Describing the Orientation between the Two Tensors Determined for the Zirconium Halides and Fluorozirconates[a]

compounds	δ_{ISO} (ppm)	C_Q (MHz)	η_Q	δ_{CSA} (ppm)	η_{CSA}	α (deg)	β (deg)	γ (deg)
$ZrCl_4$	844(4)	14.65(20)	0.48(2)	385(30)	0.66(9)	2(6)	76(4)	4(3)
$ZrBr_4$	1185(11)	13.16(70)	0.53(2)	330(21)	0.68(9)	0(6)	77(2)	4(2)
ZrI_4 (Zr1)	1690(18)	11.00(73)	0.51(12)	268(39)	0.75(31)	0(12)	73(4)	0(10)
(Zr2)	1667(5)	10.58(18)	0.60(4)	310(15)	0.90(10)	0(5)	80(2)	0(5)
ZrF_4 (Zr1)	−280(80)	29.96(47)	1.00(5)	710(325)	0.87(30)	10(9)	80(5)	165(6)
(Zr2)	−360(25)	34.70(21)	0.33(1)	260(100)	0.48(28)	65(40)	5(10)	30(40)
Ba_2ZrF_8	−190(30)	19.26(54)	0.68(2)	b	b	b	b	b
$Na_5Zr_2F_{13}$	−140(20)	16.48(14)	0.45(2)	b	b	b	b	b
Cs_2ZrF_6	−70(6)	17.74(7)	0.02(2)	b	b	b	b	b
K_2ZrF_6	−150(145)	44.71(28)	0.94(3)	b	b	b	b	b

[a] The chemical shift parameters are defined as $\delta_{ISO} = (\delta_{11} + \delta_{22} + \delta_{33})/3$, $\delta_{CSA} = \delta_{33} - \delta_{ISO}$ and $\eta_{CSA} = (\delta_{22} - \delta_{11})/\delta_{CSA}$, where δ_{ii} are the principal values of the CSA tensor defined in the sequence $|\delta_{33} - \delta_{ISO}| \geq |\delta_{11} - \delta_{ISO}| \geq |\delta_{22} - \delta_{ISO}|$. The quadrupolar parameters are defined as $C_Q = (eV_{33}Q)/h$ and $\eta_Q = (V_{11} - V_{22})/V_{33}$, where V_{ii} are the eigenvalues of the electric field gradient tensor with the convention $|V_{33}| \geq |V_{22}| \geq |V_{11}|$ (e is the electron charge, Q is the nuclear quadrupole moment and h is Planck's constant). [b] Not measured.

Chemical shift and quadrupolar parameters of the two Zr sites were obtained from a simultaneous fit of the spectra recorded at these two different magnetic fields.[28−34] The intensity ratio of the two contribution (1:3) is slightly different from what is expected from the site multiplicities (1:2), seemingly because of longitudinal relaxation or transverse dephasing effects. Nevertheless, the ^{91}Zr resonance of highest intensity with a C_Q of 34.70 MHz is unambiguously assigned to the Zr2 site, while the remaining one with a C_Q of 29.96 MHz is assigned to the Zr1 site. It should be mentioned that these C_Q values are significantly smaller than that previously reported in reference 10 (C_Q = 53.7 MHz), but the polymorphic form and the preparation of this highly moisture-sensitive sample is not mentioned in this earlier work.

α-Ba_2ZrF_8 exhibits an orthorhombic structure built of isolated ZrF_8 bicapped trigonal prisms with a unique Zr crystallographic site (ISCD-85717).[41] As expected from the structure, fits of the Hahn echo and QCPMG static spectra (Figure 3a) indicate that the Zr local environment is far from axial symmetry (η_Q = 0.68) with a significant quadrupolar coupling value of 19.26 MHz.

The monoclinic structure of $Na_5Zr_2F_{13}$ exhibits corner-sharing ZrF_7 monocapped trigonal prims connected by pairs and contains a unique Zr crystallographic site in the asymmetric unit (ICSD-155759).[42] In this case, a quadrupolar coupling value of 16.48 MHz and an asymmetry parameter η_Q = 0.45 were obtained from the fits of the ^{91}Zr static line shape (Figure 3b).

The trigonal structure of Cs_2ZrF_6 exhibits isolated ZrF_6 octahedra with only one Zr crystallographic site in the asymmetric unit (ICSD-25598).[43] Fits of the powder patterns shown in Figure 3c give a C_Q of 17.74 MHz and a ^{91}Zr isotropic chemical shift of −70 ppm. The quadrupolar coupling tensor is found to be axially symmetric ($\eta_Q \sim 0$), consistent with the location of Zr on the special position 1a of $\bar{3}$m symmetry of the space group $P\bar{3}m1$ (No. 164). The intensities of the experimental spectrum singularities are not perfectly reproduced by the simulation (possibly because of an eventual preferred orientation of the sample's crystallites, or anisotropic longitudinal or transverse relaxational effects), but this does not affect the determination of the quadrupolar coupling parameters from the positions of the experimental singularities. The values determined here are in excellent agreement with those previously reported by Hartmann and Scheler[11] (C_Q = 17.88 MHz, η_Q = 0, and δ_{ISO} = −191 ppm relative to $Zr(C_5H_5Br)_2$ in THF corresponding to δ_{ISO} = −69.1 ppm relative to $Zr(C_5H_5Cl)_2$ in THF[44]).

The monoclinic structure of K_2ZrF_6 is built of ZrF_8 edge-sharing square antiprisms forming infinite chains along the c axis (ICSD-855).[45,46] As shown in Figure 3d, the unique Zr crystallographic site of the structure gives rise to a very broad ^{91}Zr static line shape covering a spectral range of about 1.7 MHz at 17.6 T, hence revealing a very large C_Q (C_Q = 44.71 MHz). This very large quadrupolar interaction can be related to the strong distortions of the Zr coordination polyhedron. This coordination polyhedron includes four non-bridging F atoms and four bridging ones. Two of these bridging fluorine atoms exhibit significantly longer Zr−F distances, and the F−Zr−F bond angles between them and the opposed F atoms of the square bases (107.7°) are far from the ideal value of 118.5°.

4. Discussion

Among the various factors influencing the isotropic chemical shift, the electronegativity of the neighboring atoms is known to have a major effect. This is clearly illustrated in the case of the zirconium halides for which the ^{91}Zr isotropic chemical shift covers a wide spectral range of ∼2000 ppm, ranging from −360 ppm for β-ZrF_4 to 1690 ppm for ZrI_4. As shown in Figure 4a, we observe a very good linear correlation between the ^{91}Zr isotropic chemical shift and Pauling's electronegativity (EN)[47,48] of the halogens (δ_{ISO} = −1505 EN + 5658 with n = 5 and R^2 = 0.998), and an increase of the electronegativity of the anion leads to a decrease of the ^{91}Zr chemical shift. The observed trend for isotropic chemical shift is also correctly reproduced considering the ionic

(41) LeBail, A.; Laval, J. P. *Eur. J. Solid State Inorg. Chem.* **1998**, *35*, 357–372.
(42) Herak, R. M.; Malcic, S. S.; Manojlovic, L. M. *Acta Crystallogr.* **1965**, *18*, 520–522.
(43) Bode, H.; Teufer, G. *Z. Anorg. Allg. Chem.* **1956**, *283*, 18–25.
(44) Sayer, B. G.; Hao, N.; Denes, G.; Bickley, D. J.; McGlinchey, M. J. *Inorg. Chim. Acta* **1981**, *48*, 53–55.
(45) Hoppe, R.; Mehlhorn, B. *Z. Anorg. Allg. Chem.* **1976**, *425*, 200–208.
(46) Youngman, R. E.; Sen, S. *Solid State Nucl. Magn. Reson.* **2005**, *27*, 77–89.
(47) Pauling L. *The nature of the chemical bond*, 3rd ed.; Cornell University: Ithaca, NY, 1960.
(48) James, A. M.; Lord, M. P. *Macmillan's Chemical and Physical data*; Macmillan: London, U.K., 1992.

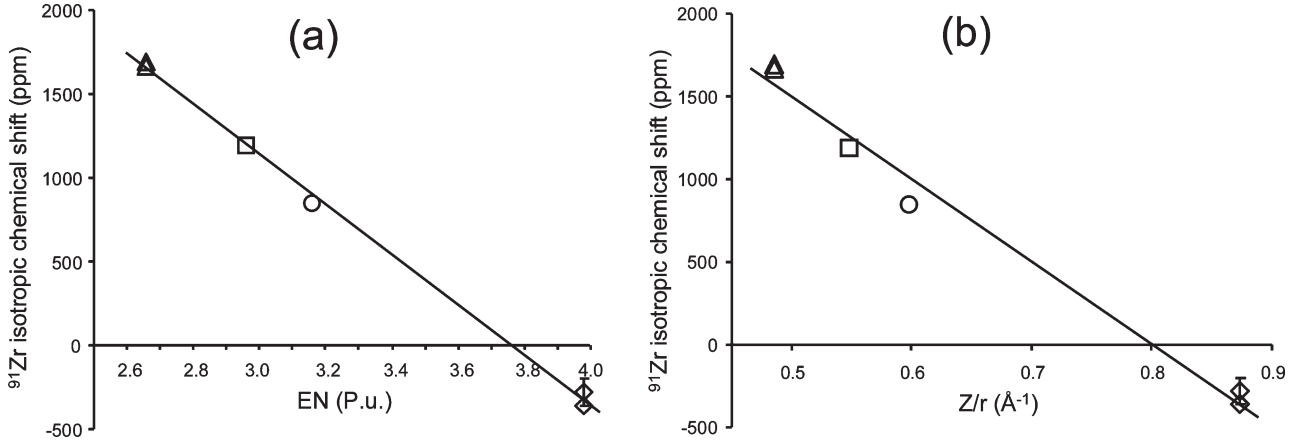

Figure 4. Evolution of the ^{91}Zr isotropic chemical shift in zirconium halides as a function of (a) the electronegativity (Pauling unit) of the halogen and (b) its anionic potential (Z/r). Triangles, squares, circles, and diamonds correspond to ZrI_4, $ZrBr_4$, $ZrCl_4$, and β-ZrF_4, respectively. Error bars are within the symbols unless otherwise specified.

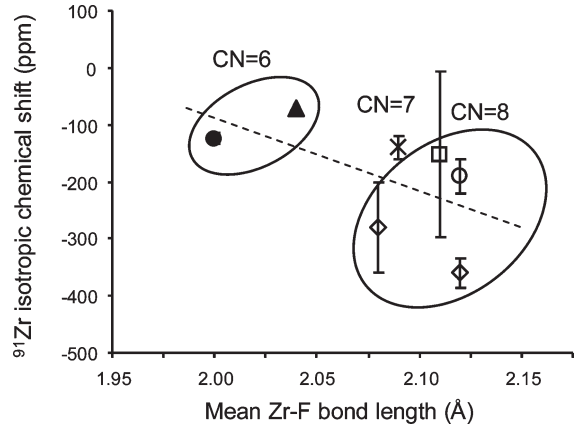

Figure 5. Variation of the ^{91}Zr isotropic chemical shift in fluorozirconates as a function of the mean Zr−F bond length. White diamonds, circles, and squares correspond to β-ZrF_4, α-Ba_2ZrF_8, and K_2ZrF_6, respectively (CN = 8). The cross corresponds to $Na_5Zr_2F_{13}$ (CN = 7). Black triangles and circles stand for Cs_2ZrF_6 and Li_2ZrF_6, respectively (CN = 6). The ^{91}Zr chemical shift value of Li_2ZrF_6 is obtained from reference 11. Error bars are within the symbols unless otherwise specified.

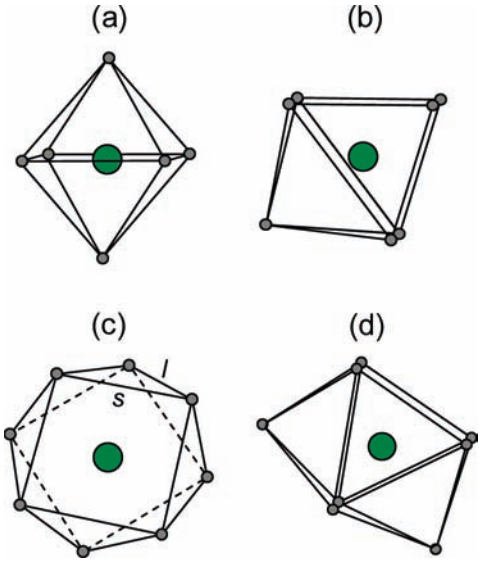

Figure 6. Representation of the various zirconium coordination polyhedra: (a) octahedron (6-fold coordination), (b) monocapped trigonal prism (7-fold coordination), (c) Archimedean antiprism, and (d) bicapped trigonal prism (8-fold coordination).

potential Z/r, where r is the ionic radius[49] of the halogen. As the anionic potential increases (i.e., the ionic radius decreases), the ^{91}Zr nucleus becomes more shielded. In this case, a linear correlation (Figure 4b) between the isotropic chemical shift and the anionic potential gives a slightly lower R^2 correlation coefficient of 0.986 ($\delta_{ISO} = -4990$ (Z/r) + 4006, $n = 5$). Since the variation of the anionic potential is only due to the ionic radii of the halogens, a good linear correlation between the ^{91}Zr isotropic chemical shift and the average Zr−X bond length is similarly obtained ($R^2 = 0.992$ and $n = 5$, not shown).

For the polycrystalline fluorozirconates, the ^{91}Zr isotropic chemical shift range only spans over ∼300 ppm, from −360 to −70 ppm for β-ZrF_4 and Cs_2ZrF_6, respectively. In this case, the ^{91}Zr isotropic chemical shift is expected to be influenced by several structural parameters, such as the zirconium coordination number, the Zr−F bond lengths, and the nature of the second neighbors. As shown in Figure 5, an increased shielding of ^{91}Zr is observed when the Zr coordination number and the mean Zr−F bond length increase. This trend is similar to that observed for other nuclei such as ^{207}Pb and ^{29}Si, for example.[50,51]

For quadrupolar nuclei like ^{91}Zr, quadrupolar parameters are also an important source of information since the electric field gradient at the nucleus is strongly sensitive to local structural distortions.[52−56] Therefore we have investigated correlations between the ^{91}Zr C_Q and the structural distortions of the Zr coordination polyhedra. In the studied compounds, the zirconium atom adopts various distinct

(49) Shannon, R. D. *Acta. Crystallogr. A* **1976**, *32*, 751–767.

(50) Fayon, F.; Farnan, I.; Bessada, C.; Coutures, J.; Massiot, D.; Coutures, J. P. *J. Am. Chem. Soc.* **1997**, *119*, 6837–6843.

(51) Skibsted, J.; Hjorth, J.; Jakobsen, H. J. *Chem. Phys. Lett.* **1990**, *172*, 279–283.

(52) Ghose, S.; Tsang, T. *Am. Mineral.* **1973**, *58*, 748–755.

(53) van der Klink, J. J.; Veeman, W. S.; Schmid, H. *J. Phys. Chem.* **1991**, *95*, 1508–1511.

(54) Engelhardt, G.; Veeman, W. J. *J. Chem. Soc., Chem. Commun.* **1993**, 622–623.

(55) Weller, M. T.; Brenchley, M. E.; Apperley, D. C.; Davies, N. A. *Solid State Nucl. Magn. Reson.* **1994**, *3*, 103–106.

(56) Padro, D.; Howes, A. P.; Smith, M. E.; Dupree, R. *Solid State Nucl. Magn. Reson.* **2000**, *15*, 231–236.

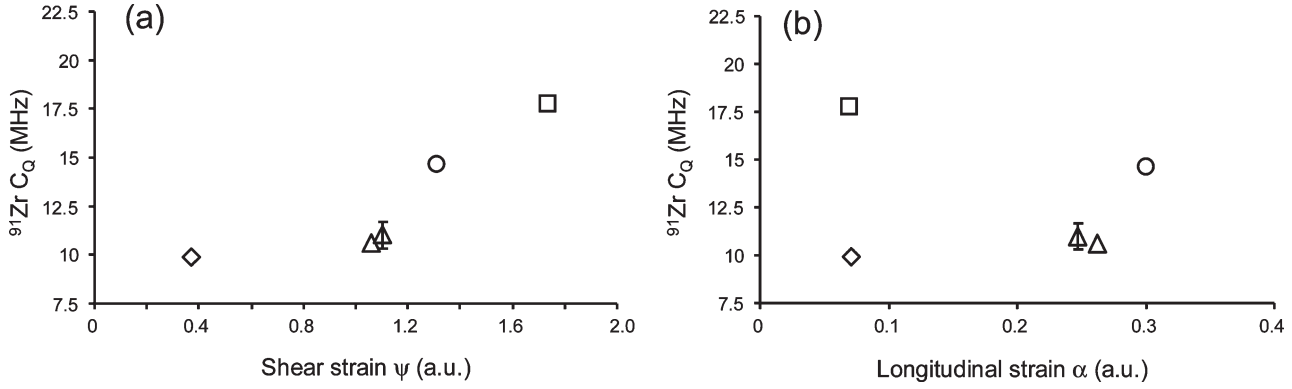

Figure 7. Evolution of the ^{91}Zr C_Q of ZrX_6 sites as a function of (a) the shear strain and (b) the longitudinal strain of the octahedron. Triangles, circles, squares, and diamonds correspond to ZrI_4 (Zr1 and Zr2 sites), $ZrCl_4$, Cs_2ZrF_6, and Li_2ZrF_6, respectively. ^{91}Zr C_Q value of Li_2ZrF_6 is obtained from reference 11. Error bars are within the symbols unless otherwise specified.

coordination polyhedra that are depicted in Figure 6: octahedron (6-fold coordination), monocapped trigonal prism (7-fold coordination), Archimedean antiprism, and bicapped trigonal prism (8-fold coordination).

To quantitatively describe the distortions from an ideal octahedron, we used the longitudinal strain α and shear strain ψ of the coordination polyhedron as suggested by Ghose and Tsang.[52] These two parameters are defined as:

$$\alpha = \sum|\ln(l_i/l_0)| \quad (1)$$

$$\psi = \sum|\tan(\theta_i - \theta_0)| \quad (2)$$

where l_i is the individual Zr−X bond length, l_0 is the ideal bond length in a perfect octahedron having the same volume as the coordination octahedron, θ_i is the individual X−Zr−X bond angle, and θ_0 the ideal bond angle (90° for an octahedron).

The longitudinal strain α is therefore related to the variation of Zr−X bond lengths, whereas the shear strain ψ measures the deviations of the X−Zr−X bond angles. The longitudinal and shear strains calculated for the ZrX_6 octahedra in $ZrCl_4$, ZrI_4, and Cs_2ZrF_6 are given in Table 1. Distortion parameters of the ZrF_6 octahedron in Li_2ZrF_6 ($\alpha = 0.071$, $\psi = 0.373$), for which a C_Q of 9.9 MHz was reported,[11] were also considered. For these ZrX_6 octahedra, we obtain a correlation between C_Q and the shear strain ψ (Figure 7a) while the plot of C_Q versus the longitudinal strain α remains more scattered (Figure 7b), as previously observed for ZrO_6 octahedra in layered zirconium phosphates[14] and TiO_6 octahedra in perovskite structures.[56]

These distortion criteria cannot be used to describe seven- and eight-fold coordinated Zr atoms. In $Na_5Zr_2F_{13}$, the zirconium coordination polyhedron has been identified as a monocapped trigonal prism where the Zr−F distance to the apical fluorine atom is significantly longer than the others. In contrast with pentagonal bipyramid, this coordination polyhedron has intrinsic deviation from spherical symmetry, which necessarily leads to a significant quadrupolar interaction.

For the 8-fold coordination polyhedra, we have applied the Poraï-Koshits and Aslanov's criteria[40] to describe the shape of the coordination polyhedra. For the Archimedean antiprism, the s/l ratio (Figure 6) can be taken as a measurement of the distortion,[40] and we introduce the distortion parameter ξ:

$$\xi = \sum|s_i/l_i - s_0/l_0| \quad (3)$$

where s_i/l_i is the ratio between the edges of the square planes and the edges of triangular faces in the distorted antiprism, s_0/l_0 being equal to 1 in the ideal antiprism.

The calculated ξ values are 0.63 and 0.40 for K_2ZrF_6 and the Zr1 site of β-ZrF_4, respectively. According to this criterion, the larger ^{91}Zr C_Q is observed for the more distorted antiprism ($C_Q = 44.71$ MHz for K_2ZrF_6 and $C_Q = 29.96$ MHz for the Zr1 site of β-ZrF_4) and the ratio between the two ξ values (1.58) is close to the ratio between the corresponding C_Q values (1.49).

For the bicapped trigonal prism, distortions of the polyhedron can be evaluated considering the set of characteristic angles δ between pairs of faces intersecting along edges of the polyhedron (see reference 40 for a detailed description). In an ideal bicapped trigonal prism, these angles are $\delta_1 = 0°$, $\delta_2 = 21.7°$, and $\delta_3 = \delta_4 = 48.2°$. For the Zr2 site of β-ZrF_4, theses angles are $\delta_1 = 3.3°$, $\delta_2 = 17.2°$, $\delta_3 = 42.8°$, and $\delta_4 = 45.0°$, while one finds the values $\delta_1 = 0°$, $\delta_2 = 24.8°$, $\delta_3 = 40.4°$, and $\delta_4 = 45.3°$ for the ZrF_8 bicapped trigonal prism in α-Ba_2ZrF_8. The average deviation from ideal δ angles is thus larger for the Zr2 site of β-ZrF_4 (4.1°) than for α-Ba_2ZrF_8 (3.4°) and accordingly, the ^{91}Zr C_Q is larger for the Zr2 site of β-ZrF_4 ($C_Q = 34.70$ MHz) than for α-Ba_2ZrF_8 ($C_Q = 19.26$ MHz). Therefore, these results suggest that the relationships between the C_Q and the distortion of the coordination polyhedron can also be extended to 8-fold coordinated zirconium sites (Archimedean antiprism and bicapped trigonal prism) using specific distortion criteria.

5. Conclusion

High magnetic field ^{91}Zr solid-state NMR spectra of zirconium halides and several fluorozirconates have been obtained using both the Hahn echo and the QCPMG sequences combined with the broadband VOCS technique. ^{91}Zr CSA and C_Q's of the Zr sites were extracted from line shape simulations of the experimental powder patterns. For the zirconium halides, the ^{91}Zr isotropic chemical shift covers a range of about 2000 ppm and shows a good correlation with both Pauling's electronegativity and ionic potential of the halogen. For the fluorozirconate samples, the Zr atoms

exhibit various coordination polyhedra, and we observe that increasing the Zr coordination number and the mean Zr−F bond length leads to an increased isotropic shielding. The ^{91}Zr C_Q's in the studied compounds range from about 10.6 to 44.7 MHz. For the 6−fold coordinated Zr sites, we report a correlation between the ^{91}Zr electric field gradient and the shear strain of the octahedron, as previously observed for ZrO_6 and TiO_6 octahedra. The relationship between the C_Q and the distortion of the Zr polyhedron has also been extended to 8-fold coordination (square antiprism and bicapped trigonal prism) using different distortion criteria. The high sensitivity of the ^{91}Zr chemical shift and quadrupolar coupling parameters to the coordination and coordination polyhedra distortions show that ^{91}Zr solid-state NMR can be used as a structural probe in more complex zirconium-based materials.

Acknowledgment. The authors thank the CNRS-PACEN Programme PCR ANSF and the Regional Council of the Region Centre for financial support. We also thank Dr. Pierre Chamelot and Dr. Pierre Florian for providing samples and Emmanuel Véron for DRX measurements. The work at LNCMI was supported by the *EuroMagNET* under EU contract n°228043.

Supporting Information Available: Additional information as noted in the text. This material is available free of charge via the Internet at http://pubs.acs.org.